

Di-photon rate enhancement in the NMSSM with nearly degenerate scalar and pseudoscalar Higgs bosons

Shoaib Munir, Leszek Roszkowski*, Sebastian Trojanowski
National Centre for Nuclear Research, Hoża 69, 00-681 Warsaw, Poland

Shoaib.Munir@fuw.edu.pl,
L.Roszkowski@sheffield.ac.uk,
Sebastian.Trojanowski@fuw.edu.pl

December 3, 2024

Abstract

We propose a scenario in the Next-to-Minimal Supersymmetric Standard Model in which its both lightest scalar and pseudoscalar Higgs bosons have masses around 125 GeV. The pseudoscalar can produce an enhanced $\gamma\gamma$ decay rate due to light higgsino-like charginos in its effective one-loop coupling to two photons. In that case, it should contribute to the $\gamma\gamma$ rate measured at the LHC, but not to the WW/ZZ decay modes. Thus a discrepancy should be observed between the rates in these two decay channels through precise measurements. However, the pseudoscalar will stay hidden behind the SM-like scalar Higgs boson in the dominant gluon fusion production mode and in order for it to be observable the $b\bar{b}h$ production mode has to be considered. We analyze the constrained NMSSM with non-universal Higgs sector parameters, and identify regions in its parameter space where the lightest pseudoscalar with mass around 125 GeV and a measurable $\gamma\gamma$ rate in the $b\bar{b}h$ mode can be obtained.

1 Introduction

Since its observation at the LHC in July 2012 [1, 2], the CMS and ATLAS collaborations have accumulated more data and updated their results on the Higgs boson. In the early results, a considerable enhancement in the $\gamma\gamma$ and ZZ rates compared to the Standard Model (SM) prediction was noted near ~ 125 GeV at the ATLAS detector. According to the CMS data, the signal strength, $\sigma/\sigma_{\text{SM}}$, was consistent with the SM prediction in the ZZ channel but an enhancement in the $\gamma\gamma$ channel was observed there as well. However, the figures from both experiments have changed in the latest results released after the collection of $\sim 20/\text{fb}$ of data [3, 4]. The signal strengths measured by the CMS have now fallen down to SM-like values in the $\gamma\gamma$ and ZZ decay channels with the mean value of the boson mass being 125.6 ± 0.64 GeV. The ATLAS collaboration, on the other hand, still reports significant excesses, $\sigma/\sigma_{\text{SM}} = 1.65 \pm 0.35$ in the $\gamma\gamma$ channel with the mass measurement yielding 126.8 ± 0.73 GeV, and $\sigma/\sigma_{\text{SM}} = 1.7 \pm 0.5$ in the ZZ channel with mass at $124.3^{+0.55}_{-0.4}$ GeV. Moreover, broad peaks consistent with a 125 GeV boson have now also been observed in the $H \rightarrow WW \rightarrow 2l2\nu$ channel at the two detectors. Importantly, the best-fit signal

*On leave of absence from the University of Sheffield, UK.

strength in this channel is very SM-like according to both CMS and ATLAS, with a measured value of 0.76 ± 0.21 at the former and of 1.01 ± 0.31 at the latter.

Since the first announcements of the discovery of the boson, there have been many attempts to interpret the observed data in light of various supersymmetric (SUSY) extensions of the SM [5, 6, 7, 8, 9, 10, 11, 12, 13, 14, 15]. In the context of the Minimal Supersymmetric Standard Model (MSSM) the observed signal can be interpreted as being due to the lightest Higgs boson of the model, h . In the MSSM constrained at the grand unification theory (GUT) scale, referred to as the CMSSM [16], h can attain a mass around the measured central value only if the SUSY-breaking scale, M_{SUSY} , is much larger than 1 TeV, while also satisfying other important phenomenological constraints. In the Next-to-Minimal Supersymmetric Standard Model (NMSSM) [17, 18] (see, e.g., [19, 20] for a review) it has been shown that either of the two lightest CP-even Higgs bosons, h_1 and h_2 , can easily be SM-like with mass around 125 GeV [21, 11]. In fact in this model it is possible to have h_1 and h_2 almost degenerate in mass around 125 GeV [9], so that the observed signal is actually a superposition of two individual peaks due to each of these, which cannot be independently resolved.

In the GUT-constrained version of the NMSSM (CNMSSM) [18, 22, 23, 24], in analogy with the CMSSM, it has been found that in order to obtain h_1 as heavy as 125 GeV, M_{SUSY} at or above 1 TeV is needed even with relevant phenomenological constraints imposed [14]. Alternatively, a SM-like h_2 with mass ~ 125 GeV is easily achievable [14]. Relaxing slightly the universality conditions by disunifying the masses of the scalar Higgs doublets m_{H_u} and m_{H_d} from the scalar mass parameter m_0 and the soft Higgs trilinear coupling parameters A_λ and A_κ from the unified soft Yukawa coupling A_0 , makes it relatively easy to obtain SM-like h_1 or h_2 around 125 GeV [25]. Here we refer to such a model with non-universal Higgs sector parameters as CNMSSM-NUHM. The scenario with mass degenerate h_1 and h_2 satisfying also other phenomenological constraints has also been pursued with much interest in the CNMSSM-NUHM [9, 10].

Even though the latest results from CMS seem to favor a SM-like Higgs boson, those from ATLAS do so only partially and it is still possible for the observed boson to be a non-standard one. The inconsistencies between the various measurements and fluctuations in the data leave ample room for speculation in this regard. Therefore, in this article, we propose a scenario, not investigated hitherto, in which the lightest pseudoscalar of the model, a_1 , is almost degenerate in mass with the lightest ~ 125 GeV scalar, h_1 . Such a_1 will thus be partially responsible for an enhanced signal rate in the $\gamma\gamma$ channel but, being a pseudoscalar, will not contribute to the WW and ZZ channels:

$$R_{\gamma\gamma}^Y(\text{obs}) \equiv \frac{\sigma_{h_i}^Y}{\sigma_{\text{SM}}^Y} = R_{\gamma\gamma}^Y(h_1) + R_{\gamma\gamma}^Y(a_1) \simeq 1 + R_{\gamma\gamma}^Y(a_1) \quad \text{and} \quad R_{WW/ZZ}^Y(\text{obs}) = R_{WW/ZZ}^Y(h_1) \simeq 1. \quad (1)$$

In the above equation the signal rate is defined as

$$R_{\gamma\gamma}^Y(h_i) = \frac{\sigma(Y \rightarrow h_i)}{\sigma(Y \rightarrow h_{\text{SM}})} \times \frac{BR(h_i \rightarrow X)}{BR(h_{\text{SM}} \rightarrow X)}, \quad (2)$$

where $X = \gamma\gamma, ZZ/WW$ and h_{SM} is a SM Higgs boson with the same mass as h_i . Y implies the various possible Higgs production modes at the LHC, which include gluon fusion (ggh), vector boson fusion (VBF), Higgs-strahlung off a vector boson (Wh/Zh)¹ and associated production off a heavy quark ($t\bar{t}h/b\bar{b}h$). Our proposed solution is made possible by the contribution of a light higgsino-like chargino, χ_1^\pm , to the effective couplings of a_1 to a $\gamma\gamma$ pair. h_1 is still SM-like in this scenario due to a significant singlet component even though $\tan\beta$ can take fairly large values [26]. Since this

¹We note here that the VBF and Wh/Zh production modes are irrelevant for a pseudoscalar Higgs boson.

scenario is compatible with a SM-like scalar Higgs boson, it is not in conflict with the recent CMS measurements in the ZZ mode [27, 28] which disfavor the pure pseudoscalar hypothesis.

We stress that in our scenario the enhancement in the $\gamma\gamma$ rate due to the a_1 contribution will not be visible in the ggh production mode. The reason is that the small enhancement achievable in $\frac{BR(a_1 \rightarrow X)}{BR(h_{SM} \rightarrow X)}$ ratio will be negligible in this production mode due to the very small effective coupling of the pseudoscalar to gluons which is dominated by the top quark loop. Such an enhancement can, therefore, only be noticeable in the $b\bar{b}h$ production mode which will also get enhanced proportionally to the $b\bar{b}$ decay width of a_1 . For this reason we shall investigate this particular mode of Higgs production here. We emphasize the fact that a measurement of the signal rate due to the $b\bar{b}h$ production channel, $R_{\gamma\gamma}^{bb}$, which is extremely subdominant for a SM Higgs and is therefore generally ignored, becomes enhanced by $\tan^2\beta$ in SUSY models and could lead to a very clear signature of our proposed scenario. Furthermore, a difference of the mass measurements in the $\gamma\gamma$ and ZZ modes would also provide a hint for mass degenerate h_1 and a_1 . Such a degeneracy would imply that the signal observed in the $\gamma\gamma$ channel should in fact be interpreted as the ‘sum’ of two individual peaks due to h_1 and a_1 , while the peaks in the ZZ/WW modes are because of h_1 alone.

We explore regions of the CMSSM-NUHM parameter space favoring such a scenario, expecting that a discrepancy between $\gamma\gamma$ and WW/ZZ rates will be seen by CMS and ATLAS collaborations with a focussed analysis of the $b\bar{b}h$ production mode. We investigate the impact of other important experimental constraints on the regions of the model parameter space accommodating this scenario. They include the limits from direct SUSY searches released by ATLAS with $\sim 20/\text{fb}$ of data as well as from the dark matter (DM) relic density measurements. We also require the corresponding parameter space to satisfy the recently announced positive $BR(B_s \rightarrow \mu^+\mu^-)$ measurement from the LHCb collaboration.

The article is organized as follows. In Sec. 2 we discuss the possibility of observing an enhancement in the $\gamma\gamma$ rate at the LHC due to a $\sim 125\text{ GeV}$ pseudoscalar Higgs. In Sec. 3 we outline the model parameter space. In Sec. 4 we describe the experimental constraints applied in our scans, present our numerical results and discuss their salient features. We summarize our findings in Sec. 5.

2 Enhancement in the observed $\gamma\gamma$ rate due to a light pseudoscalar

In this section we present some analytical details of our proposed NMSSM scenario in which the correlation between the $\gamma\gamma$ and WW/ZZ rates can be altered. One way to achieve this is with mass degenerate lightest doublet-like scalar Higgs, h_1 , and lightest singlet-like pseudoscalar, a_1 .

2.1 The pseudoscalar mass

We first discuss the conditions that are necessary to obtain a ~ 125 singlet-like a_1 which couples to two photons through loops of fermions and charginos only. Starting from the 2×2 pseudoscalar mass matrix (after rotating away the Goldstone mode) [19], one can obtain the approximate expression,

$$m_{a_1}^2 \simeq -3\kappa s A_\kappa^{\text{SUSY}} - \frac{M_{P,12}^4}{M_{P,11}^2}. \quad (3)$$

In the above equation $M_{P,12}^2 \simeq \lambda(A_\lambda^{\text{SUSY}} - 2\kappa s)v$ is the off-diagonal entry of the pseudoscalar mass matrix, where $v \equiv \sqrt{v_u^2 + v_d^2} \simeq 174\text{ GeV}$, with v_u and v_d being the vacuum expectation values (vevs) of the u -type and d -type Higgs doublets, respectively, and $A_{\lambda/\kappa}^{\text{SUSY}}$ denoting $A_{\lambda/\kappa}$ at M_{SUSY} .

$M_{P,11}^2 \simeq \mu_{\text{eff}} B_{\text{eff}} \tan \beta$, with $\mu_{\text{eff}} \equiv \lambda s$ (s being the vev of the singlet field S), $B_{\text{eff}} \equiv A_\lambda^{\text{SUSY}} + \kappa s$ and $\tan \beta \equiv v_u/v_d$, is the diagonal term corresponding to the mass-squared of the doublet-like heavy pseudoscalar, a_2 . The leading term in eq. (3) implies that, for positive κ , which we will assume here, the condition of the positivity of $m_{a_1}^2$ depends predominantly on the relative signs of μ_{eff} and A_κ . We explain the effects of negative and positive μ_{eff} in the following.

For $\mu_{\text{eff}} < 0$ (and therefore negative s , assuming positive λ), the first term in eq. (3) is positive if $A_\kappa > 0$ at M_{SUSY} . The second term then gives a negative correction to $m_{a_1}^2$ depending on the sizes of $M_{P,12}^4$, which is positive definite, and $M_{P,11}^2$, which must be positive for a non-tachyonic a_2 , requiring in turn $B_{\text{eff}} < 0$. Assuming that the correct m_{a_1} is achieved by adjusting the free parameters in the leading term, the negative contribution from the second term should be kept close to zero. This would require $M_{P,11}^2 \gtrsim M_{P,12}^4$. For given $\tan \beta$ and μ_{eff} , $M_{P,11}^2$ is driven by the magnitude of B_{eff} , in order to enhance which A_λ (which is bounded from above by $\kappa|s|$) should take smaller values. However, A_λ at M_{SUSY} runs upwards from its GUT value with falling negative A_0 owing to the contribution from relevant term in its renormalization group equation (RGE) [19]. Hence increasing negative A_0 diminishes the difference between the two terms in B_{eff} , reducing its size and in turn driving $M_{P,11}^2$ closer to zero. At the same time $M_{P,12}$, which is a sum of $2\kappa|s|$ and A_λ , grows as A_λ increases, as opposed to $M_{P,11}^2$. Consequently, the ratio $\frac{M_{P,12}^4}{M_{P,11}^2}$ in eq. (3) grows with decreasing A_0 and, for large negative values of the latter, can result in negative $m_{a_1}^2$. Note also that the running of A_κ in turn depends dominantly on A_λ . A_κ runs upwards with A_λ as long as the latter is negative. When A_λ turns positive A_κ runs in the opposite direction, owing to its RGE. Thus A_κ in the leading term in eq. (3) will have somewhat constrained GUT scale values that can yield correct m_{a_1} . On the other hand, for $\mu_{\text{eff}} > 0$, the two terms in B_{eff} are both positive and the cancellation described above does not occur.

In summary, the net effect of the interplay between various Higgs sector parameters is that for negative μ_{eff} the values of A_0 at the GUT scale are bounded from below by the condition of the physicality of a_1 . This constraint on A_0 causes a slight tension between m_{h_1} and m_{a_1} , since it is well known that to obtain h_1 which is SM-like with mass ~ 125 GeV large negative values of A_0 are required for $M_{\text{SUSY}} \sim 1$ TeV. For positive μ_{eff} there is no such tension because A_0 is relatively free to take values that give large negative A_t at M_{SUSY} , as long as the correct a_1 mass can be achieved by adjusting other free parameters.

2.2 $\gamma\gamma$ decay of the pseudoscalar

Besides a singlet-like a_1 with mass similar to that of the experimentally observed boson, this scenario also requires a low mass, $m_{\chi_1^\pm}$, of the lightest chargino. The effective coupling of a pseudoscalar a_i , with $i = 1, 2$, to two photons (see, e.g., [29, 30]), is dominated by such a light chargino in the loops and can, therefore, be approximated by

$$C_{a_i}^{\text{eff}}(\gamma\gamma) \simeq \frac{g_{a_1\chi_1^\pm\chi_1^\pm}}{\sqrt{\sqrt{2}G_F} m_{\chi_1^\pm}} A_{1/2}^{a_i}(\tau_i), \quad (4)$$

where $\tau_i = \frac{m_{a_i}^2}{4m_{\chi_1^\pm}^2}$. For $\tau_i \leq 1$, which is applicable here, with $m_{a_i} \simeq 126$ GeV and the light chargino obeying the lower limit, $m_{\chi_1^\pm} > 94$ GeV [31], the form-factor $A_{1/2}^{a_i}(\tau_i) = \frac{1}{\tau_i} \arcsin^2 \sqrt{\tau_i}$ [32] in the above equation lies in the range

$$1 < A_{1/2}^{a_i}(\tau_i) \lesssim 1.2. \quad (5)$$

The coupling of a_i to charginos in eq. (4) can be written, following the notation of [19], as

$$g_{a_i \chi_1^\pm \chi_1^\pm} = i \left[\frac{\lambda}{\sqrt{2}} P_{i3} \sin \theta_U \sin \theta_V - \frac{g_2}{\sqrt{2}} (P_{i2} \cos \theta_U \sin \theta_V + P_{i1} \sin \theta_U \cos \theta_V) \right], \quad (6)$$

where θ_U, θ_V are the mixing angles for rotating the chargino interaction states to mass eigenstates, and P_{ij} are the entries of the mixing matrix that diagonalizes the pseudoscalar mass matrix. When the pseudoscalar weak eigenstates A_i^{weak} are expressed in the basis (H_{dI}, H_{uI}, S_I) [19], P_{i1} corresponds to H_{dI} , P_{i2} to H_{uI} and P_{i3} to S_I .

The first term in eq. (6) implies that $\sin \theta_{U,V} \simeq 1$ (yielding a higgsino-like χ_1^\pm), $P_{13} \simeq 1$ and that larger values of λ are needed in order to enhance $C_{a_1}^{\text{eff}}(\gamma\gamma)$ for the singlet-like a_1 . Under these conditions, the coupling of a_1 to $b\bar{b}$ is naturally suppressed due to the tiny H_{dI} component. On the other hand, for the doublet-like pseudoscalar, a_2 , an enhancement in $C_{a_2}^{\text{eff}}(\gamma\gamma)$ requires either $\cos \theta_U \sin \theta_V$ or $\sin \theta_U \cos \theta_V$ to be non-negligible. This can be realized only in a very limited region of the parameter space where $M_2 \simeq \mu_{\text{eff}}$ and not too large in order to keep $m_{\chi_1^\pm}$ low. Moreover, in such a case, the mixing angles in the chargino sector read

$$\theta_{U,V} \simeq \arctan \left[\frac{\pm 2M_W^2 \frac{1-\tan^2 \beta}{1+\tan^2 \beta} - 2\sqrt{(M_W^2 + \mu_{\text{eff}}^2)^2 - \mu_{\text{eff}}^4}}{\sqrt{2} M_W \mu_{\text{eff}} (1 + \tan \beta)} \right], \quad (7)$$

where m_W is the mass of W boson. The sign of the first term implies that the enhancement can only be seen when a_2 has a leading H_{dI} component so that the term in eq. (7) proportional to $\sin \theta_U \cos \theta_V$ is dominant. Evidently, in such a case the $a_2 b\bar{b}$ coupling and in turn $\text{BR}(a_2 \rightarrow b\bar{b})$ will also get enhanced. Consequently, a contribution from a_2 will provide no significant excess in the $\gamma\gamma$ signal rate, defined in eq. (2).

The above explanation also precludes such a scenario in the MSSM, where the pseudoscalar, A , is doublet-like. Besides, as noted in [33, 34], in the MSSM in order to obtain a lightest CP-even Higgs boson, h , with mass around 125 GeV, m_A is required to be $\gtrsim 300$ GeV, which is the so-called decoupling regime of the model. On the other hand, while it is also possible to have a ~ 125 GeV H , the heavier CP-even Higgs boson of the MSSM, this can only be achieved for $95 \text{ GeV} < m_A < 110 \text{ GeV}$, in a tiny portion of the ‘non-decoupling regime’. This region is, moreover, disfavored by the constraints from flavor physics [35, 36].

In the fully constrained version of the NMSSM, unification of A_κ and A_0 at the GUT scale introduces tension between the masses of h_1 and a_1 , not allowing both to acquire values $\lesssim 125$ GeV simultaneously. There, in order to obtain the correct h_1 mass, large negative values of A_0 are necessary so that the mixing term ($\frac{X_t}{M_{\text{SUSY}}} \simeq \frac{A_t}{M_{\text{SUSY}}}$) can be maximized. A light a_1 , on the other hand requires small A_κ at M_{SUSY} , which in turn implies small A_κ at the GUT scale, owing to the effects of running. Moreover, small values of μ_{eff} , necessary to obtain light higgsino-like charginos, additionally limit the running of A_t in the CNMSSM [14]. Therefore, to obtain a SM-like ~ 125 GeV h_1 and a pseudoscalar with a similar mass and a non-negligible $\gamma\gamma$ rate one has to look beyond the MSSM and the CNMSSM, hence we analyse the CNMSSM-NUHM here.

Through the mechanism explained above, a more precise measurement of the reduced effective coupling, $C_{a_1}(\gamma\gamma) \equiv \frac{C_{a_1}^{\text{eff}}(\gamma\gamma)}{C_{h_{\text{SM}}}^{\text{eff}}(\gamma\gamma)}$, can yield an effective limit on the mass of the lighter chargino through²

$$C_{a_1}(\gamma\gamma) \simeq \lambda \times \frac{130 \text{ GeV}}{m_{\chi_1^\pm}}, \quad (8)$$

²Assuming a singlet-like a_1 , which implies $P_{13} \simeq 1$, and a higgsino-like χ_1^\pm so that $\sin \theta_{U,V} \simeq 1$.

for $m_{a_1} \simeq 125$ GeV. The bound obtained on the mass of χ_1^\pm is also an effective upper limit on the mass of the lightest neutralino, χ ($\equiv \chi_1^0$).

Having described the mechanism for enhancing the $\gamma\gamma$ decay rate of a_1 , we now discuss the actual quantity used for comparison with the experimentally observed $\gamma\gamma$ rate. In terms of the reduced effective couplings, $C_{a_1}(\gamma\gamma)$ and $C_{a_1}(dd)$, of a_1 to $\gamma\gamma$ and $b\bar{b}$, respectively, the signal rate, given in eq. (2), can be rewritten, specifically for the aforementioned associated production mode with a $b\bar{b}$ pair in the final state, as

$$R_{\gamma\gamma}^{bb}(a_1) = C_{a_1}^2(dd) C_{a_1}^2(\gamma\gamma) \frac{\Gamma_{h_{SM}}^{\text{total}}}{\Gamma_{a_1}^{\text{total}}} \simeq |P'_{11}|^2 \lambda^2 \tan^2 \beta \left(\frac{130 \text{ GeV}}{m_{\chi_1^\pm}} \right)^2 \left(\frac{1}{\Gamma_{a_1}^{\text{total}}/\Gamma_{h_{SM}}^{\text{total}}} \right), \quad (9)$$

where $|P'_{11}| \simeq \left| \frac{\lambda(A_\lambda^{\text{SUSY}} - 2\kappa s)v}{\mu(A_\lambda^{\text{SUSY}} - \kappa s)\tan\beta} \right|$ and $\Gamma_{h_{SM}}^{\text{total}}$ denoting the theoretical value of the total width of a SM Higgs boson with the same mass as a_1 . Note that while larger values of $\tan\beta$ are preferred by $C_{a_1}^2(dd)$ in the first equality in the above equation (and also $C_{h_1}^2(dd)$ in the corresponding equation for $R_{\gamma\gamma}^{bb}(h_1)$), there is a further dependence on $\tan\beta$ in $\Gamma_{h_{SM}}^{\text{total}}/\Gamma_{a_1}^{\text{total}}$ which is not as straightforward.

In the following section we will use eqs. (8) and (9) to obtain an effective upper limit on $m_{\chi_1^\pm}$ and the mass of χ , m_χ , in our model under consideration.

3 The CNMSSM-NUHM

In the fully constrained NMSSM universality conditions are imposed on the dimensionful parameters at the GUT scale. This leads to a unified gaugino mass parameter, $m_{1/2}$, in the model Lagrangian, a unified scalar soft SUSY-breaking mass parameter, besides m_0 and A_0 , to which A_λ and A_κ are also unified. These three parameters are thus the only free parameters in the CNMSSM besides the dimensionless Higgs coupling λ which is taken as an input parameter at M_{SUSY} , given the correct value of the mass of Z boson, m_Z .

In the partially unconstrained version of the model, the CNMSSM-NUHM, the soft masses of the Higgs fields, m_{H_u} , m_{H_d} and m_S , as well as the soft trilinear coupling parameters A_λ and A_κ are taken as free parameters at the GUT scale, instead of assuming their unification with m_0 and A_0 , respectively. Through the minimization conditions of the Higgs potential the three mass parameters m_{H_u} , m_{H_d} and m_S at the electroweak scale can be traded for the dimensionless singlet triple-coupling κ and the parameters μ_{eff} and $\tan\beta$. The model is thus defined in terms of the following eight continuous input parameters:

$$m_0, m_{1/2}, A_0, \tan\beta, \lambda, \kappa, \mu_{\text{eff}}, A_\lambda = A_\kappa.$$

The unification of A_λ and A_κ at the GUT scale assumed here is in general not necessary in the CNMSSM-NUHM. In fact, one can argue that the restriction on A_0 for $\mu_{\text{eff}} < 0$ and the resultant tension between m_{h_1} and m_{a_1} discussed in the previous section can be relaxed by not imposing such a condition. In that case, the affect of large A_λ can be counter-balanced by increasing A_κ independently, thus still yielding physical a_1 solutions. However, this unification condition has minimal impact on the allowed parameter space of the model for our purpose, since, as we shall see later, we can still exploit the interesting phenomenology of the model while keeping the free parameters to a minimum. This is also consistent with the fully constrained version of the model we studied earlier [14], where A_κ and A_λ are set equal to A_0 at the GUT scale even though $m_S \neq m_0$.

In the CNMSSM-NUHM, the upper limit on $m_{\chi_1^\pm}$ and m_χ , as discussed in the previous section, can be obtained from Fig. 1, where $C_{a_1}(\gamma\gamma)$ and $R_{\gamma\gamma}^{bb}(a_1)$ are shown as functions of $m_{\chi_1^\pm}$ in (a) and (b), respectively. For all points in the plots we assume $122 \text{ GeV} < m_{h_1, a_1} < 130 \text{ GeV}$.

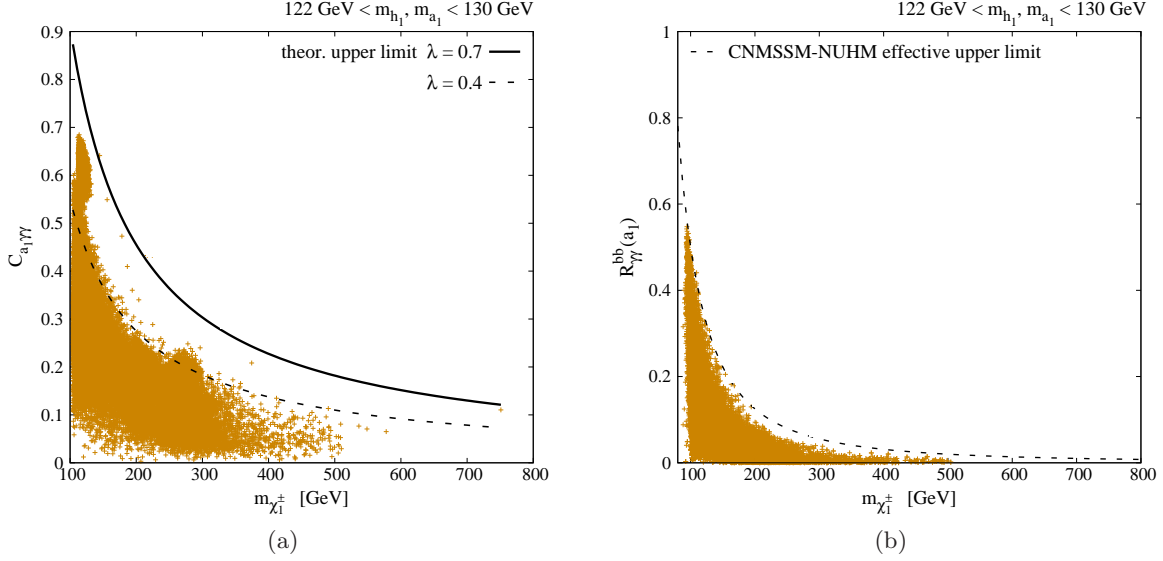


Figure 1: (a) Distribution of points obtained in our scan of the CNMSSM-NUHM parameter space in the $(m_{\chi_1^\pm}, C_{a_1}(\gamma\gamma))$ plane. The dashed line shows the effective upper limit observed in the scan. The solid line is based on a perturbative upper limit on λ and is shown for comparison. (b) Distribution of points in the $(m_{\chi_1^\pm}, R_{\gamma\gamma}^{bb}(a_1))$ plane. The dashed line shows the effective upper limit observed in our scan.

4 Methodology and results

We perform scans of the parameter space of CNMSSM-NUHM requiring the masses of h_1 and a_1 to be 125.5 GeV, with the theoretical and experimental errors taken in quadrature as 3 GeV around this mean. We impose the latest 95% confidence level (CL) exclusion limit on SUSY provided by the ATLAS collaboration [37].³ We additionally include Gaussian likelihoods for the most significant b -physics observables, with their measured mean values and errors taken as:

- $\text{BR}(B_s \rightarrow \mu^+ \mu^-) = (3.2_{-1.2}^{+1.5} \pm 0.32) \times 10^{-9}$,
- $\text{BR}(B_u \rightarrow \tau \nu) = (1.66 \pm 0.66 \pm 0.38) \times 10^{-4}$,
- $\text{BR}(\overline{B} \rightarrow X_s \gamma) = (3.43 \pm 0.22 \pm 0.21) \times 10^{-4}$ and
- $\Delta M_{B_s} = (17.72 \pm 0.04 \pm 2.4) \text{ ps}^{-1}$.

For testing the compatibility of the regions of interest against the direct detection cross section, σ_p^{SI} , we use the XENON100 90% CL exclusion limits [38]. Note that we neglect the a_μ constraint here, since it is well known that the regions where correct a_μ can be obtained in the parameter spaces of SUSY models with unification of squark and slepton soft masses are strongly disfavored by the direct SUSY searches at the LHC [39, 14, 7].

The numerical analysis was performed using the BayesFITS package which engages several external, publicly available tools: MultiNest [40] for sampling of the CNMSSM-NUHM parameter

³These limits were originally published assuming the CMSSM. However, it has been verified in [14, 7] that they have negligible dependence on the Higgs sector parameters and are, therefore, applicable to any R-parity conserving SUSY model with unified m_0 and $m_{1/2}$.

space; NMSSMTools v3.2.4 [41] for computing SUSY mass spectrum, Higgs BRs and reduced couplings, as well as ΔM_{B_s} for a given NMSSM point; SuperIso v3.3 [42] for calculating $\text{BR}(\bar{B} \rightarrow X_s \gamma)$, $\text{BR}(B_s \rightarrow \mu^+ \mu^-)$ and $\text{BR}(B_u \rightarrow \tau \nu)$. DM observables such as the relic density and σ_p^{SI} are calculated with MicrOMEGAs v2.4.5 [43].

As noted in the previous section, the scenario under consideration requires low values of μ_{eff} giving a light higgsino-like χ_1^\pm and correspondingly a χ with significant higgsino component. In fact, the CNMSSM-NUHM parameter space conforming to this scenario can be divided into three main regions depending on the composition of χ : i) the Focus Point (FP) region, ii) the higgsino region and iii) the singlino-higgsino region. Below we discuss the results for each of these regions separately. We note here that in all our results we show points with neutralino relic density, $\Omega_\chi h^2$, lying in the $\pm 2\sigma$ range, $0.087 < \Omega_\chi h^2 < 0.137$, after taking into account 10% error on the theoretical calculation. Also, we use slightly extended range of the allowed Higgs mass, $122 \text{ GeV} < m_{h_1, a_1} < 130 \text{ GeV}$, compared to the mass measurements of the observed boson at the LHC in order to allow larger values of theoretical errors. Finally, for all the points considered, h_1 is always SM-like, with $R_{\gamma\gamma}^{bb}(h_1) \simeq 1$ and $R_{ZZ/WW}^{bb}(h_1) \simeq 1$.

4.1 The focus-point region

A light neutralino with mixed bino-higgsino composition can generate correct DM relic density, $\Omega_\chi h^2$, in the so called focus-point (FP) region of minimal SUSY models in general [44]. We observed in our preliminary scans that this region better satisfies the constraints from XENON100 and $\text{BR}(b \rightarrow s \gamma)$ measurement with $\mu_{\text{eff}} < 0$, so we shall pursue this case here. In Fig. 2a we show the region in the $(m_0, m_{1/2})$ plane generating a light a_1 ($122 \text{ GeV} \leq m_{a_1} \leq 130 \text{ GeV}$) and χ with a dominant bino and a small higgsino component. In the figure light blue squares correspond to points with $1 < R_{\gamma\gamma}^{bb}(h_1 + a_1) \leq 1.15$ and green squares to points with $1.15 < R_{\gamma\gamma}^{bb}(h_1 + a_1) \leq 1.3$. We see that while large values of m_0 are favored in order to enhance the mass of h_1 , $m_{1/2}$ is typically low, which is necessary for producing a mixed bino-higgsino χ . This region, however, lies very close to the current 95% CL exclusion limit from ATLAS (also shown in the plot) and should potentially be tested soon.

In Fig. 2b we show the favored ranges of the A_0 and $\tan \beta$ parameters. $\tan \beta$ is almost always $\gtrsim 5$ to allow enhancement in the $h_1 b \bar{b}$ coupling in our considered Higgs production mode, as noted earlier. However, we see in the figure that for high positive A_0 $\tan \beta$ is limited to small values, $\lesssim 15$. The reason is that large $\tan \beta$ results in an enhanced Yukawa coupling of h_1 to $b \bar{b}$ and $\tau \bar{\tau}$. Consequently A_λ runs downwards rapidly from its GUT scale value (we shall see below that large positive A_0 coincides with negative A_λ) to more negative values at M_{SUSY} . This in turn causes A_κ to run upwards from its GUT scale value, raising m_{a_1} beyond its desired value. The effective upper bound on $\tan \beta$ is relaxed for lower $|A_0|$, when the running is slower.

In Fig. 2c we show the distribution of the parameters A_0 and $A_\kappa = A_\lambda$ at the GUT scale. We notice that A_0 stops at much smaller negative values than it would be expected to take in order to maximize m_{h_1} . This is due to the same reason as explained in Sec. 2. The main contribution to m_{a_1} comes from the leading term in eq. (3). Since in this region we assume $\mu_{\text{eff}} < 0$, A_0 is strongly bounded from below in order to minimize the affect of the second term there. Such negative A_0 , by causing positive A_λ to run upwards, also pushes A_κ to somewhat large positive values at the GUT scale resulting in its small positive values at M_{SUSY} , since it runs in the opposite direction to A_λ . This is also the reason why no points are visible in the region with negative A_κ and negative A_0 , but one can see some points with positive A_κ and positive A_0 . Finally, for negative A_κ large positive A_0 can be reached, since such values of A_0 drive positive A_λ at the GUT scale downwards, which in turn causes A_κ to run upwards to positive values at M_{SUSY} .

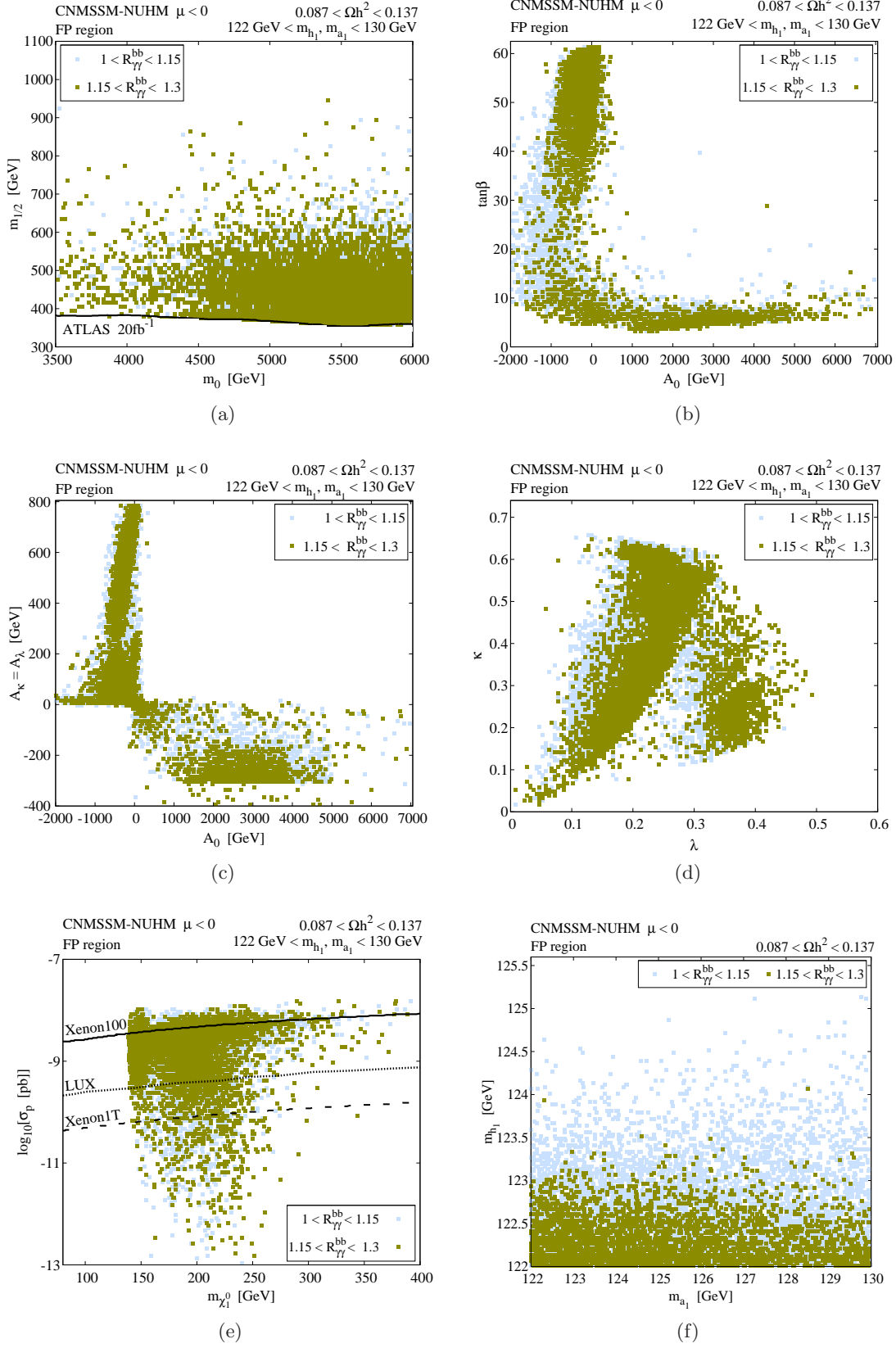


Figure 2: (a)-(d) Ranges of CNMSSM-NUHM parameters corresponding to the FP region. (e) σ_p^{SI} obtained for this region as a function of m_{χ} . (f) Ranges of m_{h_1} and m_{a_1} obtained in this region. See text for details.

Fig. 2d shows the ranges of λ and κ corresponding this scenario. While κ is widely distributed, the allowed range of λ is subject to a three-way tension. Large λ is favored in order to obtain an enhancement in the coupling of a_1 to χ_1^\pm but the condition to obtain a SM-like h_1 , on the other hand, prefers smaller values. The small-to-intermediate range of λ seen in the figure is then a result of the compromise between these two conditions and, additionally, of the requirement to achieve the desired m_{a_1} by generating s ($= \mu_{\text{eff}}/\lambda$) of the correct size.

In Fig. 2e we show how the points in the FP region yielding such a scenario fare against the XENON100 limits. Also shown in the figure are the actual 90% CL exclusion limits from XENON100 as well as the 90% CL limits expected from the LUX [45] and XENON1T [46] experiments. Note that m_χ is bounded from below by the ATLAS limit on $m_{1/2}$ in this region as it is bino-dominated. We see that a majority of the allowed points with an enhanced $\gamma\gamma$ rate lie below the XENON100 line. Most of this region, however, lies above the LUX limit, while the XENON1T data should be able to test almost all of it. Fig. 2f shows the allowed masses of h_1 and a_1 in this region. We see that m_{h_1} is always lighter than 124 GeV, which is a consequence of the not very large values of negative A_0 allowed in this region, as discussed above. a_1 , on the other hand, can easily have a mass around 125 GeV.

Overall, we notice only slight enhancement, up to $\sim 25\%$ in the $\gamma\gamma$ rate compared to the SM expectation in this region of the CNMSSM-NUHM parameter space. The reason being that $m_{\chi_1^\pm}$ is not allowed to take small enough value due to the lower bound on the mass of χ discussed above ($m_{\chi_1^\pm} \simeq \mu_{\text{eff}} > m_\chi$). $\text{BR}(B_s \rightarrow \mu^+ \mu^-)$ in this region varies between 2×10^{-9} and 5.5×10^{-9} , which is within 2σ of the experimentally measured value 3.2×10^{-9} , taking into account the theoretical error (as in [14]). On the other hand, $\text{BR}(b \rightarrow s\gamma)$ takes values between 3.1×10^{-4} and 3.7×10^{-4} and hence is always close to the experimental value. This region, owing mainly to the facts that m_{h_1} finds it difficult to reach the experimentally observed value and that the reduced $\gamma\gamma$ rate of a_1 barely exceeds 0.25, is the least favored of the three regions explored here.

4.2 The higgsino region

A nearly pure higgsino-like neutralino can generate large enough $\Omega_\chi h^2$ only if $m_\chi \simeq \mu_{\text{eff}} \sim 1$ TeV [7], but such high values of μ_{eff} will not yield the desired enhancement in the $a_1 \rightarrow \gamma\gamma$ rate. Therefore, in order to obtain a sizeable enhancement one has to relax the condition on neutralino relic density (thereby allowing low μ_{eff} and, therefore, $\Omega_\chi h^2$ to be too low). One can assume that a neutralino contributes only partially to the relic abundance of the universe beside some other DM candidate. In that case $\Omega_\chi h^2 = \xi \Omega_{\text{total}} h^2$, where ξ is the fraction of the total relic abundance produced by χ and $\Omega_{\text{total}} h^2 = 0.112$. Another possibility is that the entire relic abundance is due to an alternative DM candidate particle in the model. Often considered examples of such an additional/alternative DM candidate are gravitino (see, e.g., [47] for recent analyses in the MSSM) and/or axino [48]. The first (second) of these candidates is (not) tightly constrained by Big Bang Nucleosynthesis but both are likely to be allowed in this region due to the low neutralino yield at freeze-out.

In Fig. 3a we show the region in the $(m_0, m_{1/2})$ plane generating a light a_1 and a higgsino-like χ . Light blue squares correspond to points with $1 < R_{\gamma\gamma}^{bb}(h_1 + a_1) \leq 1.15$, green squares to points with $1.15 < R_{\gamma\gamma}^{bb}(h_1 + a_1) \leq 1.3$, red squares to points with $1.3 < R_{\gamma\gamma}^{bb}(h_1 + a_1) \leq 1.45$ and green squares to points with $1.45 < R_{\gamma\gamma}^{bb}(h_1 + a_1)$. Large values of m_0 are preferred in order to enhance m_{h_1} through radiative corrections from the SUSY sector. $m_{1/2}$ also takes large values in order to minimize the bino component of χ with large $\mu_{\text{eff}}-m_{1/2}$ splitting.

In Fig. 3b the favored ranges of $\tan\beta$ and A_0 parameters are shown. We see that the enhancement in $R_{\gamma\gamma}^{bb}(h_1 + a_1)$ decreases as $\tan\beta$ increases. The reason for this is as follows. The

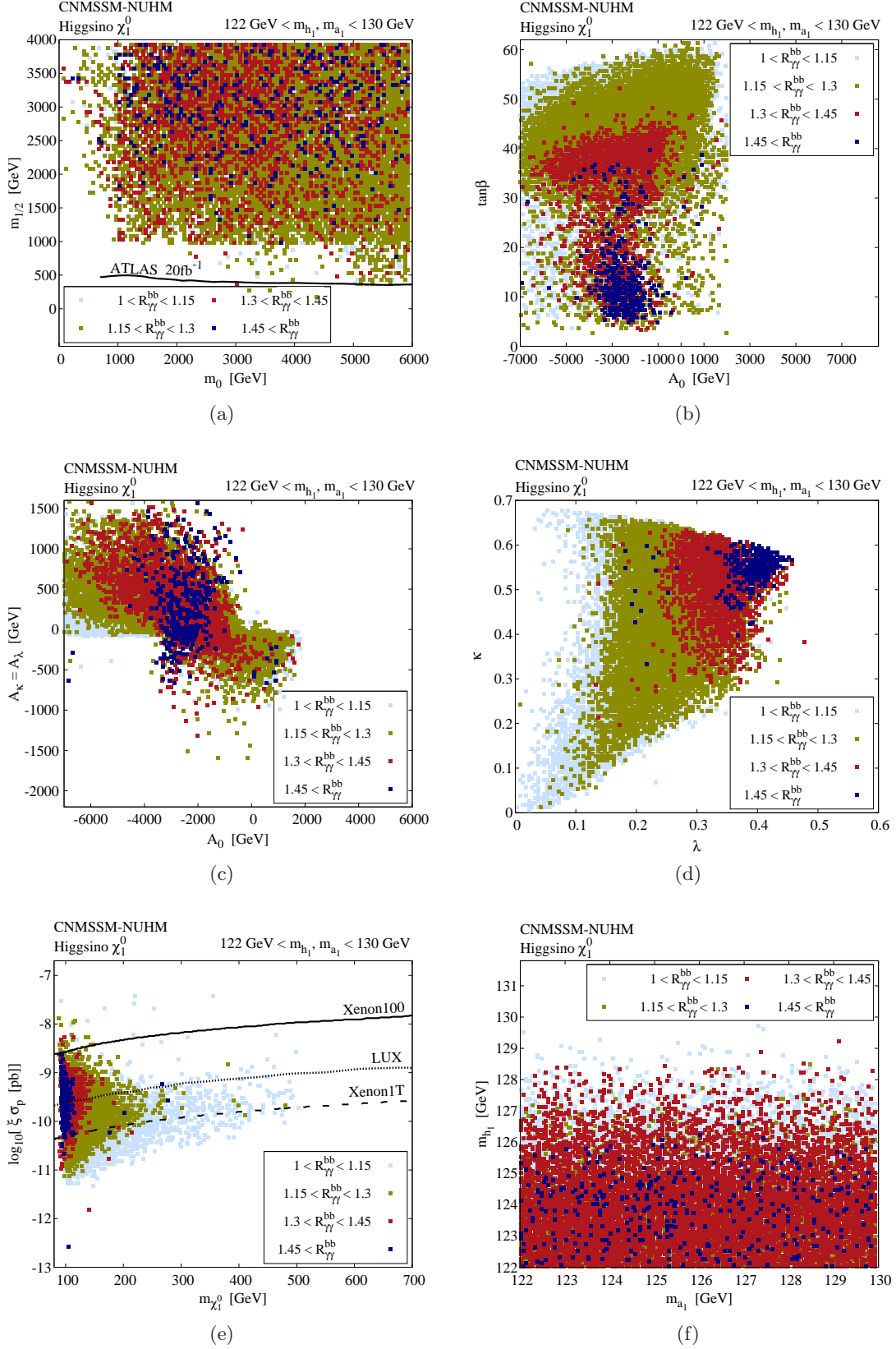


Figure 3: (a)-(d) Ranges of CNMSSM-NUHM parameters corresponding to the higgsino region. (e) $\xi \sigma_p^{SI}$ obtained for this region as a function of m_χ , where $\xi = \Omega_\chi h^2 / \Omega_{\text{total}} h^2$. (f) Ranges of m_{h_1} and m_{a_1} obtained in this region. See text for details.

enhancement in $R_{\gamma\gamma}^{bb}(a_1)$ grows with λ , according to eq. (9). However, large values of λ can only give correct m_{h_1} for not too large values of $\tan\beta$. This is because larger values of $\tan\beta$ result in an enhanced Yukawa coupling of h_1 to $b\bar{b}$ and $\tau\bar{\tau}$. This will make A_λ run upwards faster from its GUT scale value, which in turn causes A_κ to run downwards to larger negative values. That will result in a decrease in m_{h_1} , since it has a significant singlet component, while m_{a_1} increases. We point out here that an opposite affect of $\tan\beta$ was noted in the FP region due to the fact that there A_0 was positive which made A_λ and A_κ run in the opposite directions to those here.

Since for this region $\mu_{\text{eff}} > 0$, the effective constraint on A_0 from A_λ applicable in the FP region is relaxed here and larger values of negative A_0 are allowed so that m_{h_1} can be maximized. The interdependence of A_0 and $A_\lambda = A_\kappa$ is further illustrated by Fig. 3c. A_κ can take much bigger positive values at the GUT scale, even though it ought to be negative at M_{SUSY} . Moreover, a considerable number of points is visible for negative A_κ and negative A_0 up to ~ -2 TeV in contrast with the FP region. The reason is, again, the fact that here negative A_0 makes A_λ run upwards between the GUT scale and M_{SUSY} and since the latter is negative it also drives A_κ upwards to smaller negative values. Naturally then, negative A_0 should not be too large or A_κ at M_{SUSY} will be driven positive. For positive A_κ only large negative A_0 values are allowed because A_λ is also positive now and so the running of A_κ switches to downward direction. Positive A_0 solutions are also possible, as in the FP region, as long as they don't yield positive A_κ at M_{SUSY} .

In Fig. 3d the ranges of the parameters λ and κ favored by our proposed scenario are shown for this region. While κ is as widely distributed as in the FP region, comparatively slightly larger values of λ are possible in this region since s is more free to vary owing to the less constrained A_κ . In Fig. 3e we show the distribution of the points in the $(m_\chi, \xi\sigma_p^{\text{SI}})$ plane for this region.⁴ Almost all the points obtained in this region lie below the XENON100 line and a portion of these points even lies below the projected XENON1T line. Since χ is almost purely higgsino here, the smaller its mass the bigger the enhancement in $R_{\gamma\gamma}^{bb}(a_1)$ is generated. Moreover, this region corresponds to large values of m_0 and $m_{1/2}$ so that the squarks and gluinos are always much heavier than the current LHC reach. Nevertheless, as discussed earlier, a more precise measurement of $R_{\gamma\gamma}^{bb}$ could still introduce limits on m_χ and $m_{\chi_1^\pm}$. Such derived upper limits are, therefore, especially interesting from the experimental point of view.

Finally, as a result of larger allowed values of negative A_0 , h_1 as heavy as 129 GeV can be obtained in this region, as can be seen in Fig. 3f. a_1 mass is evenly distributed in the defined range, almost always showing a large enhancement in the $\gamma\gamma$ rate. Finally, compared to the FP region, a majority of points in this region show a big enhancement, up to $\sim 50\%$ above the SM expectation, in the $\gamma\gamma$ rate in this region. We also note here that both $\text{BR}(B_s \rightarrow \mu^+\mu^-)$ and $\text{BR}(b \rightarrow s\gamma)$ always lie around their respective SM values.

4.3 The singlino-higgsino region

This region is defined by χ being an admixture of a large higgsino component and a smaller but important singlino component. Owing to the significant singlino component (20%–30%) the neutralino will interact very weakly with matter and will thus result in large relic abundance unless it has a small mass and consequently large annihilation cross-section. In Fig. 4a we see the distribution of this region in the $(m_0, m_{1/2})$ plane. The color assignment of the points is the same as in the higgsino region. Large values of m_0 and intermediate values of $m_{1/2}$ are favored, again, for allowing a higgsino-like neutralino with smaller positive μ_{eff} . In Fig. 4b we see that once again

⁴The figure assumes that χ is only responsible for a small portion of the observed relic abundance. For the points obtained in the scan $\xi \leq 0.05$.

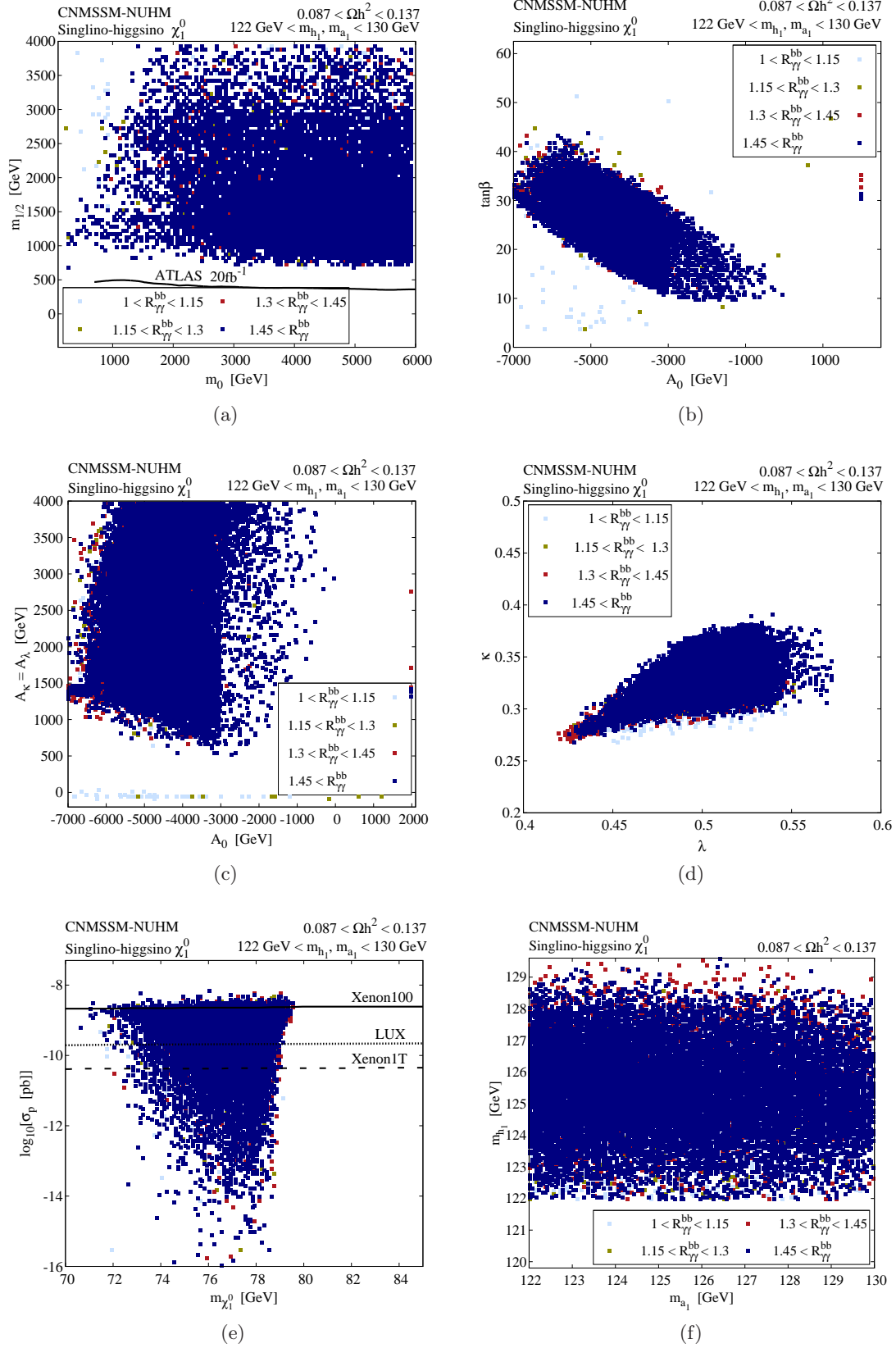


Figure 4: (a)-(d) Ranges of CNMSSM-NUHM parameters corresponding to the singlino-higgsino region. (e) σ_p^{SI} obtained for this region as a function of m_{χ} . (f) Ranges of m_{h_1} and m_{a_1} obtained in this region. See text for details.

$\tan\beta$ spans a fairly wide range but its small to intermediate values are favored by $R_{\gamma\gamma}^{bb}(a_1)$, for the same reasons as in the higgsino region. A_0 almost always takes large negative values, in order to maximize m_{h_1} . In contrast with the higgsino region, there are hardly any points corresponding to positive A_0 .

In Fig. 4c we show the distribution of points in the (A_0, A_κ) plane and in Fig. 4d in the (λ, κ) plane. The observed range of κ is smaller compared to the previous regions while that of λ is larger. This is in fact the main feature distinguishing this region from the higgsino region in terms of the parameter space of the model. Larger values of λ and small values of κ are required to maximize the singlino component of χ , as the 5×5 term in the neutralino mass matrix is equal to $2\kappa s$ ($\equiv 2\kappa\mu_{\text{eff}}/\lambda$). Hence the smallness in κ has to be compensated by slightly larger values of A_κ compared to the previous two regions, as noted in Fig. 4c, for obtaining the correct m_{a_1} . Finally, like the other two regions, the largest enhancement in $R_{\gamma\gamma}^{bb}(a_1)$ is obtained for largest possible values of λ .

In Fig. 4e we show the $(m_\chi, \sigma_p^{\text{SI}})$ plane for this region. A large number of points satisfying the XENON100 limit lies below the projected 90% CL XENON1T limit. Note also that since much smaller m_χ and consequently $m_{\chi_1^\pm}$ is favored by this region compared to the other two, almost all the points below the XENON100 line have a highly enhanced $R_{\gamma\gamma}^{bb}(a_1)$, since χ_1^\pm also appears in the denominator of eq. (9). This is also the reason why such points are achievable even with relatively small values of $\tan\beta$, as seen in Fig. 4b earlier. This region is thus the one yielding maximum enhancement, up to $\sim 60\%$ or so, in $R_{\gamma\gamma}^{bb}(h_1 + a_1)$ out of the three regions discussed here and is, therefore, the most favorable for all.

In Fig. 4f we show the distribution of m_{h_1} versus that of m_{a_1} . We note that this region yields mostly larger m_{h_1} compared to the previous two regions, which is due to the combined effects of large negative A_0 as well as larger allowed values of λ . Another distinguishing feature of this region is that h_2 can also be almost mass degenerate with h_1 and a_1 , implying in that case a ‘triple degeneracy’ among the Higgses. Again, while mass degenerate h_1 and h_2 can explain the enhanced $\gamma\gamma$ rate in the ggh production mode in the ATLAS data, in order to test the additional degeneracy with a_1 one will have to explore the associated production mode of Higgs with $b\bar{b}$. In the $b\bar{b}h$ production mode, such h_2 can further contribute $\sim 20\%$ of the measured $\gamma\gamma$ rate. Finally, $\text{BR}(B_s \rightarrow \mu^+\mu^-)$ in this region varies between 3×10^{-9} and 3.8×10^{-9} while $\text{BR}(b \rightarrow s\gamma)$ lies in the 2.8×10^{-4} to 3.3×10^{-4} range.

To conclude, in Fig. 5a we show the range of m_χ across all the regions for which an enhancement in $R_{\gamma\gamma}^{bb}(h_1 + a_1)$ was obtained in our CNMSSM-NUHM scan, and its compatibility with the current and expected limits on σ_p^{SI} . These regions are identified separately in Fig. 5b, again, in the $(m_\chi, \xi\sigma_p^{\text{SI}})$ plane, where the orange squares denote the FP region, dark green squares the higgsino region and brown squares the singlino-higgsino region.

5 Summary

We have proposed a scenario in the NMSSM in which the lightest pseudoscalar of the model, a_1 , as well a SM-like scalar Higgs boson, h_1 , both have masses around ~ 125 GeV. The pseudoscalar could be distinguishable from the scalar at the LHC in the associated production mode with a $b\bar{b}$ pair in the final state. This is because it will contribute significantly to the observed signal rate in the $\gamma\gamma$ channel but, since a pseudoscalar doesn’t couple to W and Z bosons, the measured rate in the WW/ZZ channels will be due only to the scalar and therefore SM-like. The observable enhancement in the $\gamma\gamma$ rate is made possible by a light chargino entering in the one-loop effective

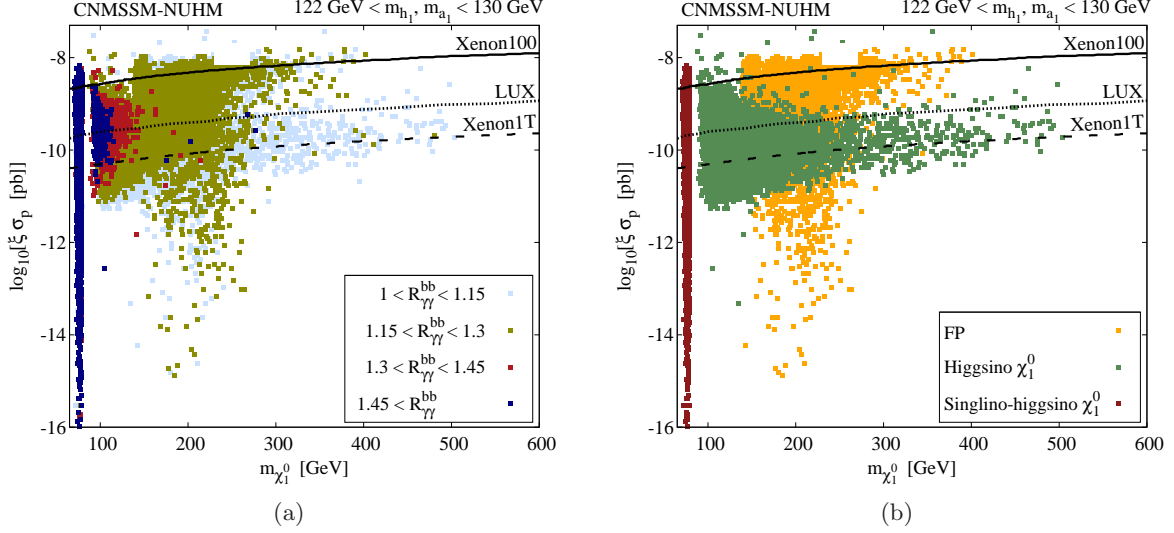


Figure 5: (a) The range of σ_p^{SI} for giving an enhancement in $R_{\gamma\gamma}^{bb}(h_1 + a_1)$ versus the neutralino mass $m_{\chi_1^0}$. Also shown are the 90% CL exclusion limits from XENON100 as well as the 90% CL limits expected from the LUX and XENON1T experiments. $\xi = \Omega_{\chi} h^2 / \Omega_{\text{total}} h^2$ when χ is almost purely higgsino but 1 otherwise. (b) The $(m_{\chi_1^0}, \sigma_p^{SI})$ plane showing the three CNMSSM-NUHM regions where $R_{\gamma\gamma}^{bb}(h_1 + a_1)$ is enhanced. Green squares denote the FP region, red squares the higgsino region and blue squares the singlino-higgsino region. $\xi = \Omega_{\chi} h^2 / \Omega_{\text{total}} h^2$ in the higgsino region, but 1 in the FP and singlino-higgsino regions.

coupling of a_1 to two photons. We have discussed the conditions necessary to obtain a_1 with the correct mass as well as an enhanced $\gamma\gamma$ rate. We have argued that due to very specific requirements on the composition of a_1 , which should be singlet-like, and of the light chargino, which should be almost purely higgsino-like, such a scenario cannot be realized in the MSSM and is extremely unlikely in the fully constrained NMSSM.

We have, therefore, analyzed the CNMSSM with the universality conditions lifted in the Higgs sector to study our proposed scenario. We have scanned the parameter space of this model in order to look for regions that can allow both χ_1^{\pm} and a_1 with the desired masses and compositions. We have found that these regions can be divided into three broad cases, based on the composition of the neutralino which, owing to the condition on χ_1^{\pm} , should also have a large higgsino component. These regions include the FP region, where χ is a bino-higgsino mixture, the higgsino region, where it is almost purely higgsino, and the singlino region, where it is higgsino-dominated but with an admixture of the singlino. The region least favored by enhancement in the $\gamma\gamma$ rate of a_1 is the FP region, where it only reaches up to $\sim 25\%$, while the most favored one is the singlino region, where the enhancement can be as high as $\sim 60\%$.

We noted, however, that such a_1 is likely to remain invisible at the LHC in the gluon-fusion production channel. The reason is that while the effective coupling of a_1 to the $\gamma\gamma$ pair gets enhanced, the effective coupling to two gluons is still highly suppressed compared to h_1 . We emphasize that a more focussed analysis of the associated Higgs production mode with $b\bar{b}$ pair, which is the least favorable production mode for a SM-like Higgs, is essential. By revealing such a pseudoscalar, this production mode could provide a clear signature of our proposed model scenario, in particular, and of beyond the SM physics, in general.

ACKNOWLEDGMENTS

The authors would like to thank Y.-L. Sming Tsai for valuable discussions and inputs. This work has been funded in part by the Welcome Programme of the Foundation for Polish Science. L.R. is also supported in part by the Polish National Science Centre grant N N202 167440, an STFC consortium grant of Lancaster, Manchester and Sheffield Universities and by the EC 6th Framework Programme MRTN-CT-2006-035505. The use of the CIS computer cluster at NCBJ is gratefully acknowledged.

References

- [1] **CMS Collaboration** Collaboration, S. Chatrchyan *et al.*, “Observation of a new boson at a mass of 125 GeV with the CMS experiment at the LHC,” [arXiv:1207.7235 \[hep-ex\]](#).
- [2] **ATLAS Collaboration** Collaboration, G. Aad *et al.*, “Observation of a new particle in the search for the Standard Model Higgs boson with the ATLAS detector at the LHC,” [arXiv:1207.7214 \[hep-ex\]](#).
- [3] twiki.cern.ch/twiki/bin/view/CMSPublic/PhysicsResultsHIG
- [4] twiki.cern.ch/twiki/bin/view/AtlasPublic/HiggsPublicResults
- [5] D. J. Chung, A. J. Long, and L.-T. Wang, “The 125 GeV Higgs and Electroweak Phase Transition Model Classes,” *Phys.Rev.* **D87** (2013) 023509, [arXiv:1209.1819 \[hep-ph\]](#). ; H. Baer, V. Barger, P. Huang, D. Mickelson, A. Mustafayev, *et al.*, “Post-LHC7 fine-tuning in the mSUGRA/CMSSM model with a 125 GeV Higgs boson,” [arXiv:1210.3019 \[hep-ph\]](#). ; Z. Heng, “A 125 GeV Higgs and its di-photon signal in different SUSY models: a mini review,” [arXiv:1210.3751 \[hep-ph\]](#). ; D. Berenstein, T. Liu, and E. Perkins, “Multiple b-jets reveal natural SUSY and the 125 GeV Higgs,” [arXiv:1211.4288 \[hep-ph\]](#). ; K. Cheung, C.-T. Lu, and T.-C. Yuan, “Diphoton Rate of the Standard-Model-Like Higgs Boson in the Extra U(1) Extended MSSM,” *Phys.Rev.* **D87** (2013) 075001, [arXiv:1212.1288 \[hep-ph\]](#). ; J. Cao, L. Wu, P. Wu, and J. M. Yang, “The Z+photon and diphoton decays of the Higgs boson as a joint probe of low energy SUSY models at LHC,” [arXiv:1301.4641 \[hep-ph\]](#).
- [6] A. Fowlie, M. Kazana, K. Kowalska, S. Munir, L. Roszkowski, *et al.*, “The CMSSM Favoring New Territories: The Impact of New LHC Limits and a 125 GeV Higgs,” *Phys.Rev.* **D86** (2012) 075010, [arXiv:1206.0264 \[hep-ph\]](#).
- [7] K. Kowalska, L. Roszkowski, and E. M. Sessolo, “Two ultimate tests of constrained supersymmetry,” [arXiv:1302.5956 \[hep-ph\]](#).
- [8] S. King, M. Muhlleitner, and R. Nevzorov, “NMSSM Higgs Benchmarks Near 125 GeV,” *Nucl.Phys.* **B860** (2012) 207–244, [arXiv:1201.2671 \[hep-ph\]](#). ; J. Cao *et al.*, “A SM-like Higgs near 125 GeV in low energy SUSY: a comparative study for MSSM and NMSSM,” *JHEP* **1203** (2012) 086, [arXiv:1202.5821 \[hep-ph\]](#). ; D. A. Vasquez *et al.*, “The 125 GeV Higgs in the NMSSM in light of LHC results and astrophysics constraints,” [arXiv:1203.3446 \[hep-ph\]](#). ; J. Rathsmann and T. Rossler, “Closing the Window on Light Charged Higgs Bosons in the NMSSM,” [arXiv:1206.1470 \[hep-ph\]](#). ; D. Das, U. Ellwanger, and P. Mitropoulos, “A 130 GeV photon line from dark matter annihilation in the NMSSM,” *JCAP* **1208** (2012) 003, [arXiv:1206.2639 \[hep-ph\]](#). ; M. Carena, S. Gori, I. Low,

- N. Shah, and C. Wagner, “Vacuum Stability and Higgs Diphoton Decays in the MSSM,” *JHEP* **1302** (2013) 114, [arXiv:1211.6136 \[hep-ph\]](#). ; P. Bechtle, S. Heinemeyer, O. Stal, T. Stefaniak, G. Weiglein, *et al.*, “MSSM Interpretations of the LHC Discovery: Light or Heavy Higgs?,” [arXiv:1211.1955 \[hep-ph\]](#).
- [9] J. F. Gunion, Y. Jiang, and S. Kraml, “Could two NMSSM Higgs bosons be present near 125 GeV?,” [arXiv:1207.1545 \[hep-ph\]](#).
- [10] J. F. Gunion, Y. Jiang, and S. Kraml, “Diagnosing Degenerate Higgs Bosons at 125 GeV,” [arXiv:1208.1817 \[hep-ph\]](#).
- [11] R. Benbrik, M. G. Bock, S. Heinemeyer, O. Stal, G. Weiglein, *et al.*, “Confronting the MSSM and the NMSSM with the Discovery of a Signal in the two Photon Channel at the LHC,” [arXiv:1207.1096 \[hep-ph\]](#). ; K. J. Bae, K. Choi, E. J. Chun, S. H. Im, C. B. Park, *et al.*, “Peccei-Quinn NMSSM in the light of 125 GeV Higgs,” [arXiv:1208.2555 \[hep-ph\]](#). ; T. Cheng, J. Li, T. Li, X. Wan, Y. k. Wang, *et al.*, “Toward the Natural and Realistic NMSSM with and without R -Parity,” [arXiv:1207.6392 \[hep-ph\]](#). ; Z. Kang, T. Li, J. Li, and Y. Liu, “A Radiatively Light Stop Saves the Best Global Fit for Higgs Boson Mass and Decays,” [arXiv:1208.2673 \[hep-ph\]](#). ; M. Perelstein and B. Shakya, “XENON100 Implications for Naturalness in the MSSM, NMSSM and lambda-SUSY,” [arXiv:1208.0833 \[hep-ph\]](#). ; K. Schmidt-Hoberg and F. Staub, “Enhanced $h \rightarrow \gamma\gamma$ rate in MSSM singlet extensions,” *JHEP* **1210** (2012) 195, [arXiv:1208.1683 \[hep-ph\]](#). ; G. Belanger, U. Ellwanger, J. Gunion, Y. Jiang, and S. Kraml, “Two Higgs Bosons at the Tevatron and the LHC?,” [arXiv:1208.4952 \[hep-ph\]](#).
- [12] J. Cao, Z. Heng, J. M. Yang, and J. Zhu, “Status of low energy SUSY models confronted with the LHC 125 GeV Higgs data,” [arXiv:1207.3698 \[hep-ph\]](#).
- [13] G. Chalons and F. Domingo, “Analysis of the Higgs potentials for two doublets and a singlet,” [arXiv:1209.6235 \[hep-ph\]](#). ; I. Gogoladze, B. He, and Q. Shafi, “Inverse Seesaw in NMSSM and 126 GeV Higgs Boson,” [arXiv:1209.5984 \[hep-ph\]](#). ; G. Belanger, U. Ellwanger, J. F. Gunion, Y. Jiang, S. Kraml, *et al.*, “Higgs Bosons at 98 and 125 GeV at LEP and the LHC,” [arXiv:1210.1976 \[hep-ph\]](#). ; H. Dreiner, F. Staub, and A. Vicente, “General NMSSM signatures at the LHC,” *Phys.Rev.* **D87** (2013) 035009, [arXiv:1211.6987 \[hep-ph\]](#). ; T. Gherghetta, B. von Harling, A. D. Medina, and M. A. Schmidt, “The Scale-Invariant NMSSM and the 126 GeV Higgs Boson,” *JHEP* **1302** (2013) 032, [arXiv:1212.5243 \[hep-ph\]](#). ; D. E. Lopez-Fogliani, “Light Higgs and neutralino dark matter in the NMSSM,” *J.Phys.Conf.Ser.* **384** (2012) 012014. ; J. Cao, Z. Heng, L. Shang, P. Wan, and J. M. Yang, “Pair Production of a 125 GeV Higgs Boson in MSSM and NMSSM at the LHC,” [arXiv:1301.6437 \[hep-ph\]](#). ; D. Das, U. Ellwanger, and A. M. Teixeira, “LHC constraints on $M_{1/2}$ and m_0 in the semi-constrained NMSSM,” [arXiv:1301.7584 \[hep-ph\]](#). ; D. G. Cerdeno, P. Ghosh, and C. B. Park, “Probing the two light Higgs scenario in the NMSSM with a low-mass pseudoscalar,” [arXiv:1301.1325 \[hep-ph\]](#). ; N. D. Christensen, T. Han, Z. Liu, and S. Su, “Low-Mass Higgs Bosons in the NMSSM and Their LHC Implications,” [arXiv:1303.2113 \[hep-ph\]](#). ; W. Wang, J. M. Yang, and L. L. You, “Higgs boson mass in NMSSM with right-handed neutrino,” [arXiv:1303.6465 \[hep-ph\]](#). ; R. Barbieri, D. Buttazzo, K. Kannike, F. Sala, and A. Tesi, “Exploring the Higgs sector of a most natural NMSSM,” [arXiv:1304.3670 \[hep-ph\]](#).

- [14] K. Kowalska, S. Munir, L. Roszkowski, E. M. Sessolo, S. Trojanowski, *et al.*, “The Constrained NMSSM with a 125 GeV Higgs boson – A global analysis,” [arXiv:1211.1693 \[hep-ph\]](#).
- [15] L. Basso and F. Staub, “Enhancing $h \rightarrow \gamma\gamma$ with staus in SUSY models with extended gauge sector,” *Phys.Rev.* **D87** (2013) 015011, [arXiv:1210.7946 \[hep-ph\]](#). ; K. Schmidt-Hoberg, F. Staub, and M. W. Winkler, “Enhanced diphoton rates at Fermi and the LHC,” *JHEP* **1301** (2013) 124, [arXiv:1211.2835 \[hep-ph\]](#). ; K. Benakli, M. D. Goodsell, and F. Staub, “Dirac Gauginos and the 125 GeV Higgs,” [arXiv:1211.0552 \[hep-ph\]](#). ; P. Athron, S. King, D. Miller, S. Moretti, and R. Nevzorov, “Constrained Exceptional Supersymmetric Standard Model with a Higgs Near 125 GeV,” *Phys.Rev.* **D86** (2012) 095003, [arXiv:1206.5028 \[hep-ph\]](#).
- [16] G. L. Kane, C. F. Kolda, L. Roszkowski, and J. D. Wells, “Study of constrained minimal supersymmetry,” *Phys. Rev.* **D49** (1994) 6173–6210, [arXiv:hep-ph/9312272 \[hep-ph\]](#).
- [17] M. Drees, “Supersymmetric Models with Extended Higgs Sector,” *Int.J.Mod.Phys.* **A4** (1989) 3635.
- [18] J. Ellis, J. F. Gunion, H. E. Haber, L. Roszkowski, and F. Zwirner, “Higgs bosons in a nonminimal supersymmetric model,” *Phys. Rev. D* **39** (Feb, 1989) 844–869. <http://link.aps.org/doi/10.1103/PhysRevD.39.844>
- [19] U. Ellwanger, C. Hugonie, and A. M. Teixeira, “The Next-to-Minimal Supersymmetric Standard Model,” *Phys.Rept.* **496** (2010) 1–77, [arXiv:0910.1785 \[hep-ph\]](#).
- [20] M. Maniatis, “The Next-to-Minimal Supersymmetric extension of the Standard Model reviewed,” *Int.J.Mod.Phys.* **A25** (2010) 3505–3602, [arXiv:0906.0777 \[hep-ph\]](#).
- [21] U. Ellwanger, “A Higgs boson near 125 GeV with enhanced di-photon signal in the NMSSM,” *JHEP* **1203** (2012) 044, [arXiv:1112.3548 \[hep-ph\]](#).
- [22] A. Djouadi, U. Ellwanger, and A. Teixeira, “The Constrained next-to-minimal supersymmetric standard model,” *Phys.Rev.Lett.* **101** (2008) 101802, [arXiv:0803.0253 \[hep-ph\]](#)
- [23] A. Djouadi, U. Ellwanger, and A. Teixeira, “Phenomenology of the constrained NMSSM,” *JHEP* **0904** (2009) 031, [arXiv:0811.2699 \[hep-ph\]](#).
- [24] J. F. Gunion, Y. Jiang, and S. Kraml, “The Constrained NMSSM and Higgs near 125 GeV,” *Phys.Lett.* **B710** (2012) 454–459, [arXiv:1201.0982 \[hep-ph\]](#).
- [25] U. Ellwanger and C. Hugonie, “Higgs bosons near 125 GeV in the NMSSM with constraints at the GUT scale,” [arXiv:1203.5048 \[hep-ph\]](#).
- [26] M. Badziak, M. Olechowski, and S. Pokorski, “New Regions in the NMSSM with a 125 GeV Higgs,” [arXiv:1304.5437 \[hep-ph\]](#).
- [27] **CMS Collaboration** Collaboration, S. Chatrchyan *et al.*, “On the mass and spin-parity of the Higgs boson candidate via its decays to Z boson pairs,” *Phys. Rev. Lett.* **110** (2013) 081803, [arXiv:1212.6639 \[hep-ex\]](#).
- [28] A. Djouadi and G. Moreau, “The couplings of the Higgs boson and its CP properties from fits of the signal strengths and their ratios at the 7+8 TeV LHC,” [arXiv:1303.6591 \[hep-ph\]](#).

- [29] M. Spira, “QCD effects in Higgs physics,” *Fortsch.Phys.* **46** (1998) 203–284, [arXiv:hep-ph/9705337 \[hep-ph\]](#).
- [30] A. Djouadi, “The Anatomy of electro-weak symmetry breaking. II. The Higgs bosons in the minimal supersymmetric model,” *Phys.Rept.* **459** (2008) 1–241, [arXiv:hep-ph/0503173 \[hep-ph\]](#).
- [31] **Particle Data Group** Collaboration, J. Beringer *et al.*, “Review of Particle Physics (RPP),” *Phys.Rev.* **D86** (2012) 010001.
- [32] A. Djouadi, “The Anatomy of electro-weak symmetry breaking. I: The Higgs boson in the standard model,” *Phys.Rept.* **457** (2008) 1–216, [arXiv:hep-ph/0503172 \[hep-ph\]](#).
- [33] N. D. Christensen, T. Han, and S. Su, “MSSM Higgs Bosons at The LHC,” *Phys.Rev.* **D85** (2012) 115018, [arXiv:1203.3207 \[hep-ph\]](#).
- [34] M. Carena, S. Heinemeyer, O. Stl, C. Wagner, and G. Weiglein, “MSSM Higgs Boson Searches at the LHC: Benchmark Scenarios after the Discovery of a Higgs-like Particle,” [arXiv:1302.7033 \[hep-ph\]](#).
- [35] S. Scopel, N. Fornengo, and A. Bottino, “Embedding the 125 GeV Higgs boson measured at the LHC in an effective MSSM: possible implications for neutralino dark matter,” [arXiv:1304.5353 \[hep-ph\]](#).
- [36] C. Boehm, P. S. B. Dev, A. Mazumdar, and E. Pukartas, “Naturalness of Light Neutralino Dark Matter in pMSSM after LHC, XENON100 and Planck Data,” [arXiv:1303.5386 \[hep-ph\]](#).
- [37] “Search for strongly produced superpartners in final states with two same sign leptons with the atlas detector using 21 fb-1 of proton-proton collisions at sqrt(s)=8 tev,” Tech. Rep. ATLAS-CONF-2013-007, CERN, Geneva, Mar, 2013
- [38] **XENON100 Collaboration** Collaboration, E. Aprile *et al.*, “Dark Matter Results from 225 Live Days of XENON100 Data,” [arXiv:1207.5988 \[astro-ph.CO\]](#).
- [39] L. Roszkowski, E. M. Sessolo, and Y.-L. S. Tsai, “Bayesian Implications of Current LHC Supersymmetry and Dark Matter Detection Searches for the Constrained MSSM,” *Phys.Rev.* **D86** (2012) 095005, [arXiv:1202.1503 \[hep-ph\]](#).
- [40] F. Feroz, M. Hobson, and M. Bridges, “MultiNest: an efficient and robust Bayesian inference tool for cosmology and particle physics,” *Mon.Not.Roy.Astron.Soc.* **398** (2009) 1601–1614, [arXiv:0809.3437 \[astro-ph\]](#).
- [41] www.th.u-psud.fr/NMHDECAY/nmssmtools.html
- [42] A. Arbey and F. Mahmoudi, “SuperIso Relic: A program for calculating relic density and flavor physics observables in Supersymmetry,” *Comput.Phys.Commun.* **176** (2007) 367–382, [arXiv:0906.0369 \[hep-ph\]](#).
- [43] G. Belanger, F. Boudjema, A. Pukhov, and A. Semenov, “micrOMEGAs2.0: a program to calculate the relic density of dark matter in a generic model,” *Comput.Phys.Commun.* **181** (2010) 1277–1292, [arXiv:hep-ph/0607059 \[hep-ph\]](#).

- [44] K. L. Chan, U. Chattopadhyay, and P. Nath, “Naturalness, weak scale supersymmetry and the prospect for the observation of supersymmetry at the Tevatron and at the LHC,” *Phys. Rev.* **D58** (1998) 096004, [arXiv:hep-ph/9710473](#). ; J. L. Feng, K. T. Matchev, and T. Moroi, “Focus points and naturalness in supersymmetry,” *Phys. Rev.* **D61** (2000) 075005, [arXiv:hep-ph/9909334](#). ; J. L. Feng, K. T. Matchev, and F. Wilczek, “Neutralino Dark Matter in Focus Point Supersymmetry,” *Phys. Lett.* **B482** (2000) 388–399, [arXiv:hep-ph/0004043](#).
- [45] **LUX Collaboration** Collaboration, D. Akerib *et al.*, “The Large Underground Xenon (LUX) Experiment,” *Nucl.Instrum.Meth.* **A704** (2013) 111–126, [arXiv:1211.3788 \[physics.ins-det\]](#).
- [46] **XENON1T collaboration** Collaboration, E. Aprile, “The XENON1T Dark Matter Search Experiment,” [arXiv:1206.6288 \[astro-ph.IM\]](#).
- [47] S. Bailly, K.-Y. Choi, K. Jedamzik, and L. Roszkowski, “A Re-analysis of Gravitino Dark Matter in the Constrained MSSM,” *JHEP* **0905** (2009) 103, [arXiv:0903.3974 \[hep-ph\]](#). ; L. Roszkowski, S. Trojanowski, K. Turzynski, and K. Jedamzik, “Gravitino dark matter with constraints from Higgs boson mass and sneutrino decays,” *JHEP* **1303** (2013) 013, [arXiv:1212.5587 \[hep-ph\]](#).
- [48] L. Covi, J. E. Kim, and L. Roszkowski, “Axinos as cold dark matter,” *Phys.Rev.Lett.* **82** (1999) 4180–4183, [arXiv:hep-ph/9905212 \[hep-ph\]](#). ; L. Covi, H.-B. Kim, J. E. Kim, and L. Roszkowski, “Axinos as dark matter,” *JHEP* **0105** (2001) 033, [arXiv:hep-ph/0101009 \[hep-ph\]](#). ; K.-Y. Choi, L. Roszkowski, and R. Ruiz de Austri, “Determining reheating temperature at colliders with axino or gravitino dark matter,” *JHEP* **0804** (2008) 016, [arXiv:0710.3349 \[hep-ph\]](#).